Analytical solution to Scholte's secular equation for isotropic elastic media

J. Antúnez-García, D. H. Galván, J. Guerrero-Sánchez,
F. N. Murrieta-Rico, R. I. Yocupicio-Gaxiola, and S. Fuentes-Moyado

Centro de Nanociencias y Nanotecnología, Universidad Nacional Autónoma de México
Apdo. Postal 2681, Ensenada, B. C., México

Received 4 August 2020; accepted 29 September 2020

In terms of a Cauchy integrals based method, robust analytical expression was obtained to predict the unique physical solution to Scholte's slowness for all elastic and isotropic medium. In particular, it is found that at the limit where the fluid above the solid vanishes, the slowness with which the interface wave propagates corresponds, as expected, to that of a Rayleigh wave. The results show that a Scholte wave's propagation speed is less than or equal to a Rayleigh wave.

Keywords: Rayleigh wave; Scholte wave; Cauchy integrals.

PACS: 43.35.Pt; 68.35.Iv; 02.90.+p

DOI: https://doi.org/10.31349/RevMexFis.67.54

1. Introduction

Materials, in general, have different mechanical properties, and consequently, body waves propagate differently inside of them. In the scientific community, there has always been an enormous interest in studying the propagation of body waves since they offer to determine in a non-invasive or destructive way, the mechanical properties of the medium through which they travel [1–5]. Its study has allowed obtaining information on the structure and composition of our planet's various layers [6]. But they have also been of great help in seismic prospecting to locate oil deposits on land, shallow and deep waters [7].

Among the mechanical waves, the most technologically attractive are those known as interfacial waves, which emerge at the interface of two media due to the coupling of both shear and compression waves [8]. The characteristics of this type of waves, which in turn make them easy to detect, are: a) they rapidly decay in-depth, b) they propagate parallel to the interface between two media, c) they have the largest amplitude, and d) they decay more slowly than body waves. There are three types of interfacial waves [9]: a) the Stoneley wave that emerges at the interface of two solids, b) the Scholte wave that appears at a solid-fluid interface, and c) the Rayleigh wave or (surface wave) that arises in the free surface of a solid exposed to a vacuum. Although interface waves are commonly used to detect defects in the surface of materials [10, 11], they can also be used to develop biosensors, temperature sensors, pressure sensors, and humidity sensors, among others [12, 13, 13]. Due to the feasibility of the physical conditions under which Scholte waves can be excited and measured, so its characterization is very attractive for the development of technological devices with practical applications [14, 15].

Theoretically, the zeros of Scholte's secular equation determine the speed with which a wave moves at the solid/fluid interface [16]. Before discussing the complexity of solving this equation, let us consider a particular case: the Rayleigh's secular equation. This last equation was formulated for the first time by Lord Rayleigh [17], and it arises from posing the problem of the propagation of a wave (with speed C) along the free surface of an elastic and isotropic solid and is described as

$$F(C) = A(C) - B(C) = 0. \tag{1}$$

Here $A(C)$ and $B(C)$ are in terms of α and β (the compressional and shear velocities, respectively) as

$$A(C) = \left(2 - \frac{C^2}{\beta^2}\right)^2,$$

$$B(C) = 4\sqrt{1 - \frac{C^2}{\beta^2}}\sqrt{1 - \frac{C^2}{\alpha^2}}. \tag{2}$$

To find a distinct solution from the trivial one ($C = 0$) in Eq. (1), Lord Rayleigh [17] proposed to find solutions to $A(C)^2 = B(C)^2$ (known as the "rationalization method"), which will lead us to a third order polynomial. The counterpart of this procedure can be obtained by introducing the following new function

$$f(C) = A(C) + B(C). \tag{3}$$

Note that the roots of Eq. (3) *do not* correspond to the problem of the Rayleigh wave propagation, but the equality

$$F(C)f(C) = A^2(C) - B^2(C) = 0 \tag{4}$$

leads to the same polynomial as the one obtained by Rayleigh. Thus, it is evident that this procedure introduces spurious roots that come from $f(C)$. Lord Rayleigh (based on physical arguments) showed for some particular cases, that Eq. (1) has only one physically acceptable root, which should be real and with speed $C < \beta$. Later on, using the same argument as Rayleigh, Knopoff *et al.* [18] numerically

extended the solution to the entire range of physically allowable Poisson radii. However, for the case of Rayleigh's wave propagation at the interface of a viscoelastic medium, the non trivial solution to Eq. (1) is not restricted to real solutions [19]. Thus, in this last case the discrimination of solutions which come from $F(C)$ and $f(C)$ is no longer straightforward.

As discussed above, the rationalization method restates the solution to Eq. (1) in terms of a third-order polynomial, the roots of which allow a piecewise solution to be constructed [20–24]. The availability of analytical expressions for the respective complex roots may incorrectly suggest additional solutions [25] to Eq. (1). Nevertheless, due to the simplicity of the method, it has been used to investigate analytically the solutions of both Scholte and Stoneley secular Eqs. [26]. However, because these equations have a larger number of square roots terms, the polynomial order increases, and consequently, the number of spurious roots introduced also increases. For these cases, even the numerical evaluation of the roots is not an easy task, and in the case of viscoelastic media, it is practically unthinkable. Nkemzi [27] and Romeo [19], in terms of a method based on Cauchy integrals, considered Eq. (1) for both the elastic and viscoelastic cases, respectively, and demonstrated the existence of only one physical solution. Later Antúnez-García [28] would consider the same method to solve the Scholte equation for a specific range of fluid velocities, which would be extended by Vinh [29], both showing that it also has only one physical solution.

As previously shown, the Scholte secular equation's parametrization in terms of the slowness drives directly to a unique physical solution of this expression [28] without any additional assumptions; then, we propose extending those results in the full range of possible fluid velocities. Unlike the work presented by Vinh [29], the current one makes a more detailed analysis of the solution's behavior for the different speed ranges with which a wave can propagate in a fluid. So the relevance of the present work falls in obtaining a simple analytical expression to describe the slowness of the Scholte wave for all the range of possible elastic and isotropic media. We also show that the Rayleigh's wave is a singular solution (at the free surface limit) that rises specifically at the connection point of two fluid speed ranges.

The article is organized as follows: Sec. 2 is devoted to give a brief introduction of the Scholte's secular equation and the requirements for the existence of that solution. In Sec. 3, the quotient of discontinuities associated to the Scholte's secular equation are analyzed, and the continuous continuation of them for different speed ranges was established. In Sec. 4 the expression for the unique physical root of the Scholte's secular equation is obtained and particularly, it is used to recover the Rayleigh wave solution. Additionally, numerical calculations were included to test the solution of the Scholte's equation. Finally, the conclusions are presented.

2. Scholte's secular equation

In general the existence of a wave propagating through the interface of two homogeneous and isotropic semi-infinite media (exponentially decaying) was predicted by Stoneley [30]. A particular case of a Stoneley wave arises when one of those semi-infinite media becomes fluid, which is known as a Scholte wave. The speed propagation of this wave (C) is a zero of the Scholte secular equation [26, 31–33]

$$F(C) = \left[\left(2-\frac{C^2}{\beta^2}\right)^2 - 4\sqrt{1-\frac{C^2}{\beta^2}}\sqrt{1-\frac{C^2}{\alpha^2}}\right] \times \sqrt{1-\frac{C^2}{C_F^2}} + \frac{\rho_F}{\rho}\left(\frac{C}{\beta}\right)^4\sqrt{1-\frac{C^2}{\alpha^2}} = 0, \quad (5)$$

under the following physical restrictions

$$\Re e\left(\sqrt{1-\frac{C^2}{\alpha^2}}\right) > 0, \quad \Re e\left(\sqrt{1-\frac{C^2}{\beta^2}}\right) > 0, \quad \Re e\left(\sqrt{1-\frac{C^2}{C_F^2}}\right) > 0, \quad (6)$$

which ensures solutions with an exponentially decaying behavior. Here α and β are the compressional and shear velocities of elastic waves in a solid, C_F is the speed of a sound wave in a fluid, ρ and ρ_F are the densities of a solid and fluid medium, respectively. Note that the terms inside of the square brackets in Eq. (5) correspond to the Rayleigh characteristic Eq. (1). By convenience we rewrite Eqs. (5) and (6) in therms of the dimensionless variable $z = \beta^2/C^2$ and parameter $\gamma = \alpha^2/\beta^2$, $\gamma^\dagger = C_F^2/\beta^2$ as

$$F(z) = \left[\sqrt{\gamma}(2z-1)^2 - 4z\sqrt{z-1}\sqrt{\gamma z-1}\right] \times \sqrt{\gamma^\dagger z-1} + \frac{\rho_F\sqrt{\gamma^\dagger}}{\rho}\sqrt{\gamma z-1} = 0 \quad (7)$$

subject to the restrictions

$$\Re e\left(\sqrt{1-\frac{1}{\gamma z}}\right) > 0, \ \Re e\left(\sqrt{1-\frac{1}{z}}\right) > 0, \ \Re e\left(\sqrt{1-\frac{1}{\gamma^\dagger z}}\right) > 0. \quad (8)$$

For any elastic and isotropic medium α, β, and C_F are real and positive quantities. In particular, the ratio of speeds can be described in terms of Poisson's (ν) ratio as

$$\gamma^{-1} = \frac{\beta^2}{\alpha^2} = \frac{1-2\nu}{2(1-\nu)}, \quad \forall\ \nu\ \in\ 0 \le \nu < 1/2. \quad (9)$$

Thus, there are three cases for the study of the characteristic Scholte equation (7): (a) $C_F > \alpha > \beta$, (b) $\alpha > C_F > \beta$ and (c) $\alpha > \beta \geq C_F$, which will be discussed below.

3. Discontinuities of Scholte's secular equation

In general the branch points of $F(z)$ are localized along the real axes $z = 1, 1/\gamma^\dagger$ and $1/\gamma$. For each of the cases mentioned in the previous section, these branch points define two main branch cuts (see Fig. 1). For the follow discussion, we will make reference to the Rayleigh branch cut Γ_R, as the one defined by

$$\Gamma_R(t) = t, \quad \forall\, t \in 1/\gamma < t \leq 1, \tag{10}$$

which describes the discontinuities presented by the Rayleigh secular equation [28].

3.1. Case (a): $C_F > \alpha > \beta$

For this case the arcs over which the discontinuities spans (see Fig. 1a)) are

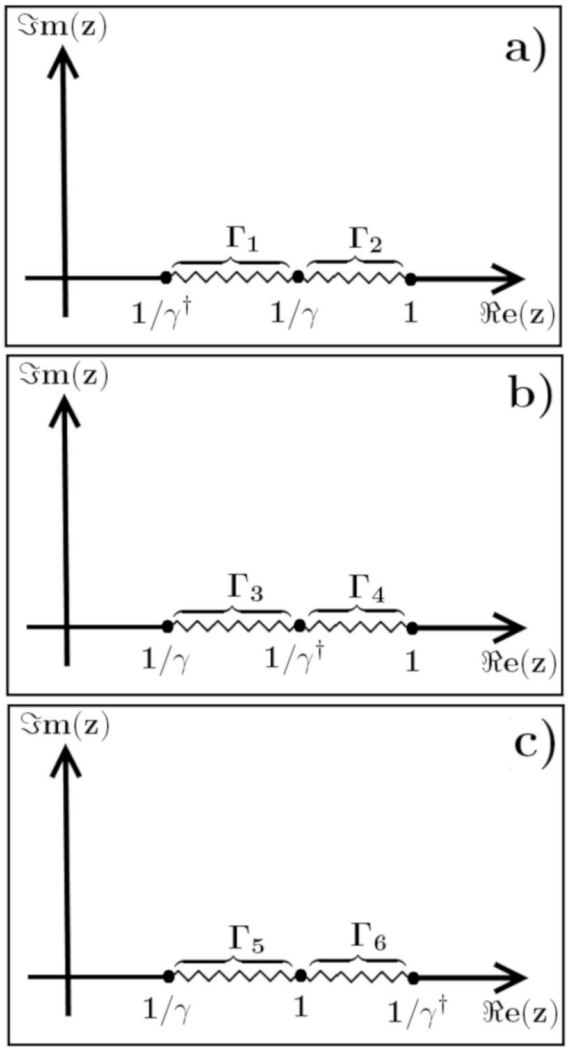

FIGURE 1. Branch cuts for the function $F(z)$ for cases in which: a) $C_F > \alpha > \beta$, b) $\alpha > C_F > \beta$ and c) $\alpha > \beta \geq C_F$.

$$\Gamma_1(t) = t, \quad \forall\, t \in 1/\gamma^\dagger \leq t \leq 1/\gamma$$
$$\Gamma_2(t) = t, \quad \forall\, t \in 1/\gamma < t \leq 1$$

The respective discontinuity quotient along each arc is described as

$$G_1(t) = \left.\frac{F^+(t)}{F^-(t)}\right|_{\Gamma_1} = \frac{1 + iH_1(t)}{1 - iH_1(t)},$$
$$G_2(t) = \left.\frac{F^+(t)}{F^-(t)}\right|_{\Gamma_2} = \frac{1 - iH_2(t)}{1 + iH_2(t)} \tag{11}$$

with the auxiliary functions

$$H_1(t) = \frac{\sqrt{\gamma^\dagger}\frac{\rho_F}{\rho}\frac{\sqrt{1-\gamma t}}{\sqrt{\gamma^\dagger t-1}}}{\sqrt{\gamma}(2t-1)^2 + 4t\sqrt{1-t}\sqrt{1-\gamma t}},$$
$$H_2(t) = \frac{4t\sqrt{1-t}\sqrt{\gamma t-1}}{\sqrt{\gamma}(2t-1)^2 + \sqrt{\gamma^\dagger}\frac{\rho_F}{\rho}\frac{\sqrt{\gamma t-1}}{\sqrt{\gamma^\dagger t-1}}}. \tag{12}$$

For the range of velocities under consideration, note that

$$\lim_{t\to 1/\gamma} G_1(t)\Big|_{\Gamma_1} = \lim_{t\to 1/\gamma} G_2(t)\Big|_{\Gamma_2} = 1$$

guarantees the continuous continuation of these functions. The limit in which the fluid vanishes ($\rho_F \to 0$) must satisfy

$$\lim_{\rho_F\to 0} H_1(t)\Big|_{\Gamma_1} = 0,$$
$$\lim_{\rho_F\to 0} H_2(t)\Big|_{\Gamma_2} = \left.\frac{1 - iH_R(t)}{1 + iH_R(t)}\right|_{\Gamma_R}. \tag{13}$$

Where Γ_R is described by Eq. (10) and

$$H_R(t) = \frac{4t\sqrt{1-t}\sqrt{\gamma t-1}}{\sqrt{\gamma}(2t-1)^2} \tag{14}$$

is the auxiliary function for the free surface limit [28]. Otherwise, the corresponding auxiliary functions are described by Eq. (12).

Moreover, it is prohibitive that $\gamma^\dagger = \gamma$, since in vacuum the mechanical waves do not propagate. However, there is not physical restriction to consider a fluid medium with density $\rho_F = \rho'$, where $0 < \rho' \ll 1$ for which exist an ϵ in the range $0 < \epsilon \ll 1$ such that $C_F = \alpha - \epsilon$. Then, at this limit we will have

$$\lim_{C_F\to\alpha-\epsilon} H_1(t)\Big|_{\Gamma_1} \neq 0,$$
$$\lim_{C_F\to\alpha-\epsilon} H_2(t)\Big|_{\Gamma_2} \neq H_R(t). \tag{15}$$

Thus, while a fluid under which the solid-fluid interface may be defined, the contribution to the fluid discontinuities will be distinct to the free-surface limit.

3.2. Case (b): $\alpha > C_F > \beta$

For a fluid under this range of velocities, the discontinuities (see Fig. 1b)) are described by

$$G_3(t) = \left.\frac{F^+(t)}{F^-(t)}\right|_{\Gamma_3} = \frac{1+iH_3(t)}{1-iH_3(t)},$$
$$G_4(t) = \left.\frac{F^+(t)}{F^-(t)}\right|_{\Gamma_4} = \frac{1-iH_4(t)}{1+iH_4(t)} \tag{16}$$

with the auxiliary functions

$$H_3(t) = \frac{\sqrt{\gamma}(2t-1)^2}{4t\sqrt{1-t}\sqrt{\gamma t-1}+\sqrt{\gamma^\dagger}\frac{\rho_F}{\rho}\frac{\sqrt{\gamma t-1}}{\sqrt{\gamma^\dagger t-1}}},$$
$$H_4(t) = \frac{4t\sqrt{1-t}\sqrt{\gamma t-1}}{\sqrt{\gamma}(2t-1)^2+\sqrt{\gamma^\dagger}\frac{\rho_F}{\rho}\frac{\sqrt{\gamma t-1}}{\sqrt{1-\gamma^\dagger t}}}, \tag{17}$$

which are defined along the arcs

$$\Gamma_3(t) = t, \quad \forall\, t \in 1/\gamma < t \leq 1/\gamma^\dagger,$$
$$\Gamma_4(t) = t, \quad \forall\, t \in 1/\gamma^\dagger \leq t \leq 1. \tag{18}$$

Here the continuous continuation and unicity of solutions is granted by

$$\lim_{t\to 1/\gamma^\dagger} G_2(t)\Big|_{\Gamma_3} = \lim_{t\to 1/\gamma^\dagger} G_3(t)\Big|_{\Gamma_4} = 1,$$

while for the limit with $\rho_F \to 0$ satisfies

$$\lim_{\rho_F\to 0} H_3(t)\Big|_{\Gamma_3} = 0, \quad \lim_{\rho_F\to 0} H_4(t)\Big|_{\Gamma_4} = \frac{1-iH_R(t)}{1+iH_R(t)} \tag{19}$$

as in the previous case. Particularly for this case, note that the Rayleigh branch cut Γ_R moves from partially screened to *unscreened* as the presence of a fluid vanishes (see Fig. 2a) and b)). Here $H_R(t)$ is described by Eq. (14). As in a previous case, it could be considered a fluid medium with density $\rho_F = \rho'' \neq \rho'$ in the range $0 < \rho'' \ll 1$ such that $C_F = \alpha+\epsilon$, with $0 < \epsilon \ll 1$. At this limit we will have

$$\lim_{C_F\to\alpha+\epsilon} H_3(t)\Big|_{\Gamma_1} \neq \lim_{C_F\to\alpha-\epsilon} H_1(t)\Big|_{\Gamma_1} \neq 0, \quad \text{and}$$
$$\lim_{C_F\to\alpha+\epsilon} H_4(t)\Big|_{\Gamma_2} \neq \lim_{C_F\to\alpha-\epsilon} H_2(t)\Big|_{\Gamma_2} \neq H_R(t). \tag{20}$$

Thus the connection of discontinuities on both cases (a) and (b) is granted trough the free-surface limit.

Contrarily to the *unscreened* Rayleigh branch cut limit, the *full-screening* of Γ_R occurs when $\gamma^\dagger \to 1$ (see Fig. 2c)) where

$$\lim_{\gamma^\dagger\to 1} H_4(t)\Big|_{\Gamma_4} = 0,$$

and

$$\lim_{\gamma^\dagger\to 1} H_3(t)\Big|_{\Gamma_3} = \frac{\sqrt{\gamma}(2t-1)^2}{4t\sqrt{1-t}\sqrt{\gamma t-1}+\frac{\rho_F}{\rho}\frac{\sqrt{\gamma t-1}}{\sqrt{1-t}}}. \tag{21}$$

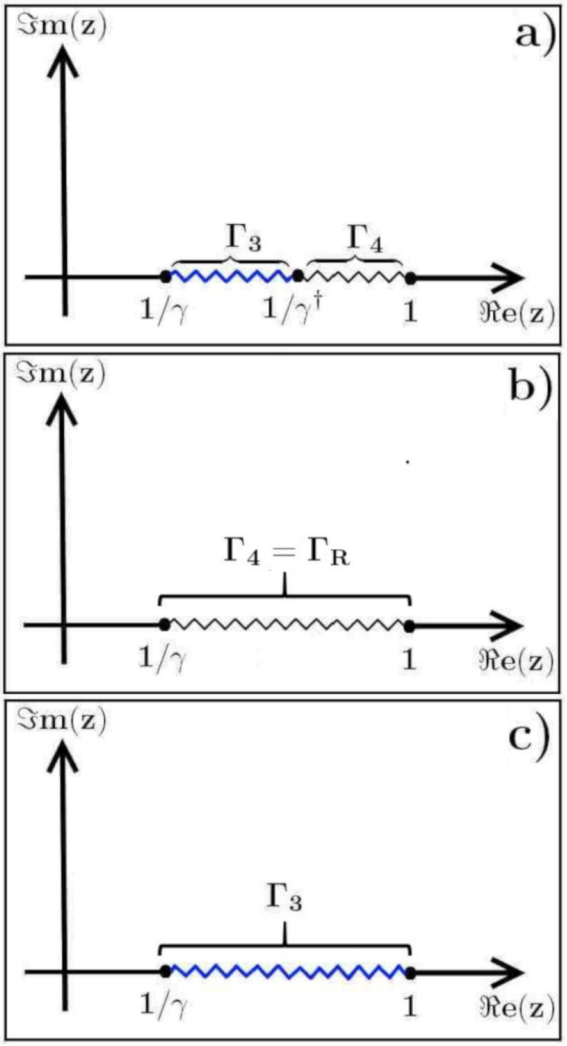

FIGURE 2. Branch cuts for the function $F(z)$ in the case that $\alpha > C_F > \beta$ for: a) the general case, b) $\rho_F \to 0$ and c) $1/\gamma^\dagger \to 1$. The branch cut colored in blue represents the fluid discontinuities' contribution to the three different cases. The cases in which Γ_R is totally unscreened and totally screened correspond to Figures b) and c) respectively.

then, the extreme values of $G_3(t)$, particularly corresponds to well-defined values

$$\lim_{\gamma^\dagger\to 1} G_3(t = 1/\gamma) = -1,$$
$$\lim_{\gamma^\dagger\to 1} G_3(t = 1) = 1.$$

3.3. Case (c): $\alpha > \beta \geq C_F$

Within this range of velocities, the discontinuities (see Fig. 1c)) are described by

$$G_5(t) = \left.\frac{F^+(t)}{F^-(t)}\right|_{\Gamma_5} = \frac{1+iH_5(t)}{1-iH_5(t)},$$

$$G_6(t) = \left.\frac{F^+(t)}{F^-(t)}\right|_{\Gamma_6} = \frac{1+iH_6(t)}{1-iH_6(t)} \tag{22}$$

along the branch cuts

$$\begin{aligned}\Gamma_5(t) &= t, \quad \forall\, t \in 1/\gamma < t \leq 1,\\ \Gamma_6(t) &= t, \quad \forall\, t \in 1 < t \leq 1/\gamma^\dagger.\end{aligned} \tag{23}$$

with the auxiliary functions

$$\begin{aligned}H_5(t) &= \frac{\sqrt{\gamma}(2t-1)^2}{4t\sqrt{1-t}\sqrt{\gamma t-1}+\sqrt{\gamma^\dagger}\frac{\rho_F}{\rho}\frac{\sqrt{\gamma t-1}}{\sqrt{1-\gamma^\dagger t}}},\\ H_6(t) &= \frac{\sqrt{\gamma}(2t-1)^2-4t\sqrt{t-1}\sqrt{\gamma t-1}}{\sqrt{\gamma^\dagger}\frac{\rho_F}{\rho}\frac{\sqrt{\gamma t-1}}{\sqrt{1-\gamma^\dagger t}}}.\end{aligned} \tag{24}$$

It should be noted that the lowest value which $1/\gamma^\dagger$ could take in this speed range is 1, which implies that not only the Rayleigh branch cut Γ_R is always screened for this case, but are also extended beyond $\Re e(z) > 1$ (See Fig. 1c)). Which is evident if it is observed that

$$\begin{aligned}\lim_{\gamma^\dagger\to 1} G_5(t)\Big|_{\Gamma_5} &= \lim_{\gamma^\dagger\to 1} G_3(t)\Big|_{\Gamma_3},\\ \lim_{\gamma^\dagger\to 1} G_6(t)\Big|_{\Gamma_6} &= 0.\end{aligned}$$

Which establishes the continuous continuation between G_3 and G_5. On the other hand, for the limit in which $\rho_F \to 0$ we have

$$\begin{aligned}\lim_{\rho^F\to 0} G_5(t)\Big|_{\Gamma_5} &= \tfrac{H_R(t)+i}{H_R(t)-i},\\ \lim_{\rho^F\to 0} G_6(t)\Big|_{\Gamma_6} &= -1.\end{aligned} \tag{25}$$

Here $H_R(t)$ is the auxiliary function defined by Eq. (14). Within this range, the discontinuities quotients are different to those obtained with the same limit in Eqs. (13) and (19). Similar expressions are obtained when $\gamma^\dagger \to 0$ is reached, however, their behavior along the arc Γ_6 is not required to be similar; this is because, in general, we do not have a physical argument to establish a linear relation between ρ and C_F.

4. The Scholte solution

Since we have guaranteed the continuous continuation of the Scholte discontinuities for the entire range of fluid velocities, we are in a position to determine the polynomial containing the zeros of Eq. (7). According to the construction 5. for the canonical solution of the Riemann problem, the polynomial with only zeros of the Scholte characteristic Eq. (7) is

$$R(z) = \frac{(2\gamma-1)\sqrt{z\gamma^\dagger}}{\sqrt{\gamma}}\left[z - \left\{\frac{2\gamma^2+(\gamma-1)^2}{4\gamma(\gamma-1)} + \frac{1}{2\gamma^\dagger} + \frac{\rho_F\gamma\left(1-\frac{\delta}{\sqrt{\gamma}}\right)}{2\rho(\gamma-1)} - I_{a,b,c}\right\}\right]. \tag{26}$$

which was obtained through the Bourniston method [34]. This method involves the expansion of Eq. (A.3) in terms of Laurent series. It should be noted that unlike previous works [19, 27, 29], the parametrization in terms of slowness conduces directly to a simple polynomial (26), and additional considerations are not necessary to solve it. In fact, directly from this polynomial is possible to have one and only one physical solution for the Scholte slowness, that is

$$z_{_{Sc}} = \left(\frac{\beta}{C_{_{Sc}}}\right)^2 = \frac{2\gamma^2+(\gamma-1)^2}{4\gamma(\gamma-1)} + \frac{1}{2\gamma^\dagger} + \frac{\rho_F\gamma\left(1-\frac{\delta}{\sqrt{\gamma}}\right)}{2\rho(\gamma-1)} - I_{a,b,c}. \tag{27}$$

Here δ is a correction parameter introduced to enhance the numerical accuracy of the Scholte root, which is a consequence of the truncation process during the Laurent series expansion (Eq. (7)). The I_a, I_b I_c terms represent the contribution of the discontinuities for the different speed ranges and are expressed in terms of Eqs. (12), (17) and (24) as

$$I_a = \frac{1}{\pi}\left[\int_{\Gamma_1}\arctan H_1(t)\,dt - \int_{\Gamma_2}\arctan H_2(t)\,dt\right], \tag{28a}$$

$$I_b = \frac{1}{\pi}\left[\int_{\Gamma_3}\arctan H_3(t)\,dt - \int_{\Gamma 4}\arctan H_4(t)\,dt\right], \tag{28b}$$

$$I_c = \frac{1}{\pi}\left[\int_{\Gamma_5}\arctan H_5(t)\,dt + \int_{\Gamma_6}\arctan H_6(t)\,dt\right]. \tag{28c}$$

4.1. The free surface limit

Contributions associated exclusively with the $\Gamma_{_R}$ branch cut, occur only at the point at which the continuous continuation of the speed range between cases (a) and (b) occurs; *i.e.*, the pole contribution. Thus, the free surface limit in terms of Eqs. (27), (28a) and (28b) corresponds to

$$\lim_{\rho_F\to 0} z_{_{Sc}} = z_{_R} = \frac{2\gamma^2+(\gamma-1)^2}{4\gamma(\gamma-1)} + \frac{1}{\pi}\int_{1/\gamma}^{1}\arctan H_{_R}(t)\,dt, \tag{29}$$

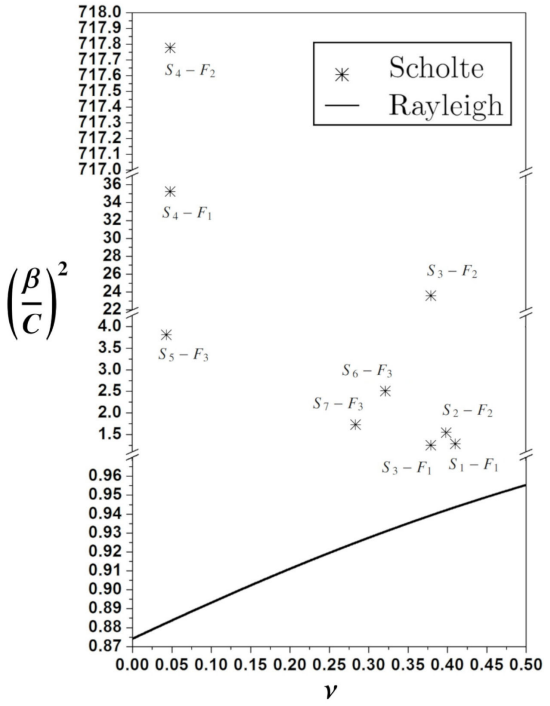

FIGURE 3. Sholte (z_{Sc}) *versus* Rayleigh (z_R) slowness as function of the Poisson's ratio.

or explicitly to

$$z_{_R} = \left(\frac{\beta}{C_{_R}}\right)^2 = \frac{2\gamma^2 + (\gamma-1)^2}{4\gamma(\gamma-1)} + \frac{1}{\pi}\int_{1/\gamma}^{1} \arctan\left(\frac{4t\sqrt{1-t}\sqrt{\gamma t-1}}{\sqrt{\gamma}(2t-1)^2}\right) dt, \qquad (30)$$

which, according to [28], describes the *exact* slowness of the Rayleigh's wave propagation. Note that the δ term is not included in this expression.

TABLE I. Input parameters for the different solid (S_i) and fluid (F_i) materials under consideration.

Material	Label	Density [Kg/m^3]	Compressional Speed [m/s]	Shear Speed [m/s]
7-A teflon[a]	S_1	2157.7	1307	503
Lucite[b]	S_2	1180	2680	1100
Silver[b]	S_3	10400	3650	1610
Berylium[b]	S_4	1870	12890	8880
Ice-1[c]	S_5	344	440	304
Ice-2[d]	S_6	442	1472	755
Ice-3[e]	S_7	637	2709	1489
Water (Distilled)[b]	F_1	998	1496	–
Air (dry)[b]	F_2	1.293	331.45	–
Sea Water[f]	F_3	1028.15	1442.45	–

[a] Reference [35]. [b] Reference [36]. [c] Values taken at sea level [37]. [d] Values taken at 5 mts depth [37]. [e] Values taken at 20 mts depth [37]. [f] Density computed at sea level, 0°C, 30 PSU salinity and 1 Atm. [38]. Compressional speed taken from Ref. [39].

4.2. Numerical Results

To numerically test the expression in Eq. (27) for different solid-fluid interfaces, we have used the parameters in Table I to illustrate the numerical derivation of the root in each of the three different fluid speed ranges. Wolfram Mathematica software was used to implement this expression numerically. The root calculated from Eq. (27) was compared with that obtained from Eq. (5) utilizing a root finder routine (provided by the software). It should be noted that not in all cases, the root finder routine was able to obtain the correct value, even when the provided value was close to the zero.

Table II (for distinct solid-fluid interfaces) shows the corrected ($\delta \neq 0$) and uncorrected ($\delta = 0$) zero values obtained. The precision of the corrected root ($z_{Sc}(\delta \neq 0)$) in terms of the exact root (z^*_{SC}) was computed using,

TABLE II. Values for the associated Poisson's ratio ν for each solid-fluid interface ($S_i - F_j$), corrected and uncorrected roots, the correction parameter δ and the precision of the corrected root Δ associated to this parameter.

Interface	ν	z_{Sc} (Uncorrected)	z_{Sc} (Corrected)	δ	Δ
$S_1 - F_1$	0.4103	1.33931	1.28279	0.54107	4.19×10^{-6}
$S_2 - F_2$	0.3987	1.63185	1.54761	0.40354	2.78×10^{-6}
$S_3 - F_1$	0.3792	1.34904	1.25176	3.702	6.6×10^{-6}
$S_3 - F_2$	0.3792	23.69205	23.59477	2857.6	2.2×10^{-7}
$S_4 - F_1$	0.04836	35.47909	35.24175	0.6781	6.3×10^{-6}
$S_4 - F_2$	0.04836	718.29634	717.77757	1144.4	1.2×10^{-5}
$S_5 - F_3$	0.0433	3.8311	3.8089	0.0112	3.18×10^{-6}
$S_6 - F_3$	0.3215	2.6407	2.5092	0.1624	5.27×10^{-6}
$S_7 - F_3$	0.2835	1.8804	1.7293	0.5555	2.36×10^{-6}

$$\Delta = F(z^*_{SC}) - F(z_{Sc}(\delta \neq 0)).$$

The results are summarized in Table II . A direct comparison of these values shows that the uncorrected root presents a relative error ϵ with respect to the corrected one between $1\% \leq \epsilon < 7\%$. Thus, even for $\delta = 0$ the predicted root presents a reasonable value. Finally, in Fig. 3, both $z_{Sc}(\delta \neq 0)$ and z_R (computed from Eq. (30)) are plotted together to compare how the Scholte slowness increases for a particular interface (and ν) in comparison with the Rayleigh slowness.

5. Conclusions

In terms of Cauchy integrals, we have obtained a robust analytic formula to predict the existence of a unique physical solution for the Scholte slowness in all range of possible elastic and isotropic media.The appropriated analysis of the discontinuities associated to the Scholte secular equation allows us to identify the free-surface limit as a pole contribution.

Unlike previous results [29], due to the secular Scholte equation's fractional-order, our results show that the truncation process involved in obtaining the rational polynomial does not allow getting an exact solution. However, our numerical results show that this solution presents a reasonable approximation to the exact value. Additionally, since slowness is the inverse of speed, the results show that a Scholte wave's propagation speed is less than or equal to that of a Rayleigh wave.

Appendix

A. The method based on Cauchy integrals

Let us consider a multivalued (or discontinuous) function $F(z)$ with a pole of finite order at infinity. If we define a Riemann function for this sheet, it would be analytical (except at infinity) with its discontinuities isolated and their branch cuts. Thus, Privalov's theory [40] allows us to rewrite this function in terms of their canonical representation, as

$$F(z) = R(z)e^{g(z)}, \tag{A.1}$$

where

$$g(z) = \frac{1}{2\pi i}\int_{\Gamma} \frac{\ln G(t)}{t-z}\, dt. \tag{A.2}$$

Here R is a rational function that contains the zeros and poles of F, G is the quotient of the lateral limits $F(t)^+$ and $F(t)^-$ along the arc Γ (which describes the branch cuts of F), and it is defined as

$$G(t) = \frac{F^+(t)}{F^-(t)}.$$

Since $e^{g(z)} \neq 0$ in all the complex domain, it is directly observed from Eq. (A.1) that R admits the representation

$$R(z) = F(z)e^{-g(z)}. \tag{A.3}$$

If the discontinuities of F are isolated at infinity, we could ensure that R contains this function's zeros. In other words, we may obtain a polynomial representation for the zeros of F in terms of a Laurent series expansion [34, 41].

1. C. B. Park, R. D. Miller, and J. Xia, Multichannel analysis of surface waves, *Geophysics* **64** (1999) 800, https://doi.org/10.1190/1.1444590.
2. J. Xia, R. D. Miller, and C. B. Park, Estimation of nearsurface shearwave velocity by inversion of Rayleigh waves, *Geophysics* **64** (1999) 691, https://doi.org/10.1190/1.1444578.
3. D. Jongmans, and D. Demanet, The importance of surface waves in vibration study and the use of Rayleigh waves for estimating the dynamic characteristics of soils, *J. Eng. Geol.* **34** (1993) 105, https://doi.org/10.1016/0013-7952(93)90046-F.
4. G. Athanasopoulos, P. Pelekis, and G. Anagnostopoulos, Effect of soil stiffness in the attenuation of Rayleigh-wave motions from field measurements, *Soil Dyn. Earthq. Eng.* **19** (2000) 277, https://doi.org/10.1016/S0267-7261(00)00009-9.
5. C. G. Lai, G. J. Rix, S. Foti, and V. Roma, Simultaneous measurement and inversion of surface wave dispersion and attenuation curves, *Soil Dyn. Earthq. Eng.* **22** (2002) 923, https://doi.org/10.1016/S0267-7261(02)00116-1.
6. A. Hanyga, Seismic Wave Propagation in the Earth (Elsevier, New York, 1985), https://doi.org/10.1016/C2009-0-09602-0.
7. K. Aki, Keiiti, and Paul G. Richards, Quantitative Seismology, 2nd ed. (University Science Books, New Jersey, 2002), https://www.ldeo.columbia.edu/~richards/Aki_Richards.html.
8. E. Flores-Mendez *et al.*, Interface Waves in Elastic Models Using a Boundary Element Method, *J. Appl. Math* **2012** (2012) 313207, https://doi.org/10.1155/2012/313207.
9. F. Luppé *et al.*, Plane evanescent waves and interface waves, in Acoustic Interactions with Submerged Elastic Structures, edited by A. Guran, A. De Hoop, D. Guicking, and F. Mainardi (World Scientific, Singapore, 2001), pp. 118-148, https://doi.org/10.1142/9789812810755_0005.
10. A. Fahr, S. Johar, M. K. Murthy and W. R. Sturrock, *Surface acoustic wave studies of surface cracks in ceramics, Review of Progress in Quantitative Nondestructive Evaluation*, edited by D. O. Thompson and D. E. Chimenti (Springer, Boston, 1984), https://doi.org/10.1007/978-1-4684-1194-2.
11. M. J. Brophy, and A. V. Granato, Surface acoustic wave studies of defects in electron irradiated GaAs, *J. Phys. Colloques* **46**

(1985) 541, https://doi.org/10.1051/jphyscol:198510120.

12. D. P. Morgan, A history of surface acoustic wave devices, *Int. J. High Speed Electron. Syst.* **10** (2000) 553, https://doi.org/10.1142/S0129156400000593.

13. J. Kondoh, Fundamentals and Applications of Surface Acoustic Wave Sensors, *IEICE ESS Fundamentals Review* **6** (2012) 166, https://doi.org/10.1587/essfr.6.166.

13. B. Liu *et al*., Surface acoustic wave devices for sensor applications, *J. Semicond.* **37** (2016) 021001, https://doi.org/10.1088/1674-4926/37/2/021001.

14. J. McLean and F. L. Degertekin, Directional scholte wave generation and detection using interdigital capacitive micromachined ultrasonic transducers, *IEEE Trans Ultrason Ferroelect Freq Control* **51** (2004) 756, https://doi.org/10.1109/TUFFC.2004.1304274.

15. M. Seidl, M. Gehring, U. Krumbein and G. Schrag, Simulation-based design of a micro fluidic transportation system for mobile applications based on ultrasonic actuation, *2018 19th International Conference on Thermal, Mechanical and Multi-Physics Simulation and Experiments in Microelectronics and Microsystems Toulouse*, 2018, edited by IEEE (IEEE, Tolouse, 2018), https://doi.org/10.1109/EuroSimE.2018.8369873.

16. J. G. Scholte. On the stoneley wave equation. *Proceedings of the Koninklijke Nederlandse Akademie van Wetenschappen* **45** (1942) 159.

17. J. W. S. Rayleigh, On waves propagated along the plane surface of an elastic solid, *Proc. London Math. Soc.* **17** (1885) 4, https://doi.org/10.1112/plms/s1-17.1.4.

18. L. Knopoff, On rayleigh wave velocity, *Bull. Seismol. Soc. Am.* **42** (1952) 307, https://pubs.geoscienceworld.org/bssa/article-pdf/42/4/307/2691698/BSSA0420040307.pdf.

19. M. Romeo, Rayleigh waves on a viscoelastic solid half-space, *J. Acoust. Soc. Am.* **110** (2001) 59, https://doi.org/10.1121/1.1378347.

20. M. Hayes, and R. S. Rivlin, A note on the secular equation for Rayleigh Waves, *Z. Angew. Math. Phys.* **13** (1962) 80, https://doi.org/10.1007/BF01600759.

21. M. Rahman, and J. R. Barber, Exact expressions for the roots of the secular equation for Rayleigh waves, *J. Appl. Mech.* **62** (1995) 250, https://doi.org/10.1115/1.2895917.

22. X. F. Liu and Y. H. Fan, A New Formula for the Rayleigh Wave Velocity, *Adv. Mater. Res*. **452** (2012) 233, https://doi.org/10.4028/www.scientific.net/AMR.452-453.233.

23. P. G. Malischewsky, Comment to "A new formula for the velocity of Rayleigh waves" by D. Nkemzi [Wave Motion 26 (1997) 199-205], *Wave Motion* **31** (2000) 93, https://doi.org/10.1016/S0165-2125(99)00025-6.

24. X. -F. Liu, and Y.-h. Fan, A New Formula for the Rayleigh Wave Velocity, *Adv. Mat. Res.* **452** (2012) 233, https://doi.org/10.1016/S0165-2125(97)00004-8.

25. P. G. Malischewsky, Comment to "A new formula for the velocity of Rayleigh" waves by D. Nkemzi [Wave Motion 26 (1997) 199-205], *Wave Motion* **31** (2000) 93, https://doi.org/10.1016/S0165-2125(99)00025-6.

26. G. Caviglia, and A. Morro, Inhomogeneous waves in solids and fluids, 1st ed. (World Scientific, Singapore, 1992).

27. D. Nkemzi, A new formula for the velocity of rayleigh waves, *Wave Motion* **26** (1997) 199, https://doi.org/10.1016/S0165-2125(97)00004-8.

28. J. Antúnez-García, Master's thesis, CICESE, Ensenada, Baja California, México (2003), http://cicese.repositorioinstitucional.mx/jspui/handle/1007/1589.

29. P. C. Vinh, Scholte-wave velocity formulae, *Wave Motion* **50** (2013) 180, https://doi.org/10.1016/j.wavemoti.2012.08.006.

30. R. Stoneley, Elastic waves at the surface of separation of two solids, *Proc. Roy. Soc. London* **106** (1924) 416, https://doi.org/10.1098/rspa.1924.0079.

31. J. G. Scholte, The range of existence of Rayleigh and Stoneley Waves, *Geophys. Suppl. Mon. Nor. R. Astron. Soc.* **5** (1947) 120, https://doi.org/10.1111/j.1365-246X.1947.tb00347.x.

32. I. A. Viktorov, Rayleigh and Lamb Waves, 1st ed. (Springer, New York, 1967).

33. E. Strick, and A. S. Ginzbarg, Stoneley-wave velocities for a fluid-solid interface, *Bull. Seismol. Soc. Am.* **46** (1956) 281.

34. E. E. Burniston, and C. E. Siewert, The use of Riemann problems in solving a class of transcendental equations, *Math. Proc. Cambridge Philos. Soc.* **73** (1973) 111, https://doi.org/10.1017/S0305004100047526.

35. P. J. Rae, and D. M. Dattelbaum, The properties of poly(tetrafluoroethylene) (PTFE) in compression, **Polymer 45** (2004) 7615, https://doi.org/10.1016/j.polymer.2004.08.064.

36. D. R. Lide, *CRC Handbook of Chemistry & Physics* 89th ed. (Taylor and Francis, London, 2008).

37. C. R. Bently, *The Ross Ice Shelf Geophysical and Glaciological Survey (RIGGS)*: Introduction and summary of measurements performed, in The Ross Ice Shelf: Glaciology and Geophysics, edited by C. R. Bentley and D. E. Hayes (American Geophysical Union, Washington D. C., 1990).

38. F. J. Millero, History of the Equation of State of Seawater, *Oceanography* **23** (2010) 18, https://doi.org/10.5670/oceanog.2010.21.

39. F. J. Millero, and T. Kubinski, Speed of sound in seawater as a function of temperature and salinity at one atmosphere, *J. Acoust. Soc. Am.* **57** (1975) 312, https://doi.org/10.1121/1.380462.

40. P. Henrici, *Computational Complex Analysis*, Vol. II, Willey, New York, (1984).

41. E. E. Burniston, and C. E. Siewert, Exact analytical solutions of the transcendental equation $\alpha \sin\zeta = \zeta$, *SIAM J. Appl. Math* **24** (1973) 460, https://www.jstor.org/stable/2099816.